Enhanced Kerr electro-optic nonlinearity and its application in controlling second-harmonic generation

Guang-Zhen Li,[1,2] Yu-Ping Chen,[1,2,*] Hao-Wei Jiang,[1,2] and Xian-Feng Chen[1,2,3]

[1]*State Key Laboratory of Advanced Optical Communication Systems and Networks, Department of Physics and Astronomy, Shanghai Jiao Tong University, 800 Dongchuan Road, Shanghai 200240, China*
[2]*Key Laboratory for Laser Plasma (Ministry of Education), IFSA Collaborative Innovation Center, Shanghai Jiao Tong University, Shanghai 200240, China*
[3]*e-mail: xfchen@sjtu.edu.cn*
**Corresponding author: ypchen@sjtu.edu.cn*

Received April 2, 2015; revised May 21, 2015; accepted May 21, 2015;
posted May 22, 2015 (Doc. ID 237276); published June 18, 2015

We proposed a new scheme of controlling second-harmonic generation by enhanced Kerr electro-optic nonlinearity. We designed a structure that can implement the cascaded Pockels effect and second-harmonic generation simultaneously. The energy coupling between the fundamental lights of different polarizations led to a large nonlinear phase shift and, thus, an effective electro-optic nonlinear refractive index. The effective nonlinearity can be either positive or negative, causing the second-harmonic spectra to move toward the coupling center, which, in turn, offered us a way to measure the effective electro-optic nonlinear refractive index. The corresponding enhanced Kerr electro-optic nonlinearity is more than three orders of magnitude higher than the intrinsic value. These results open a door to manipulate the nonlinear phase by applying an external electric field instead of light intensity in noncentrosymmetric crystals.

OCIS codes: (160.2100) Electro-optical materials; (160.4330) Nonlinear optical materials; (190.2620) Harmonic generation and mixing.
http://dx.doi.org/10.1364/PRJ.3.000168

1. INTRODUCTION

Third-order nonlinearities, though with weak third-order coefficients [1,2], exist in a medium with any symmetry [3–5]. One common way to enhance the intrinsic weak third-order nonlinearity is via cascading second-order nonlinear effects [6] because of its much higher value than the direct higher-order nonlinearity [7–9]. The Kerr electro-optic (EO) effect is connected to the appearance of the nonlinear third-order susceptibility [1]. It takes advantage of the modulation of the electric field and intrinsic nature of fast response time. Besides applications in electro-optic switching [10], electro-optical detection [11], high-speed optical shutters [12], it is also used to measure the optical third-order susceptibility of material [13]. However, the Kerr EO effect is relatively weak in noncentrosymmetric crystals for the existence of a linear EO effect [1]. Therefore, it is highly demanded to enhance Kerr EO nonlinearity and broaden its applications in noncentrosymmetric crystals.

In our previous work, we proposed a new phenomenon named cascaded polarization coupling generated in MgO doped periodically poled lithium niobate (PPLN) near its phase-matching condition [14]. However, there remains some deficiencies: (1) the experiment cannot measure the enhancement of Kerr EO nonlinearity or the effective Kerr EO coefficient; (2) the equation of phase shift did not apply for small phase-mismatching conditions; (3) it just studied the relationship between the phase shift and external electric field, and the fixed input wavelength made it difficult in practical flexibility and adjustability.

Therefore, in this paper, we mainly propose one of its potential applications in modulating second-order nonlinearity by achieving the cascaded effects and second-harmonic generation (SHG) simultaneously in a single PPLN. We also deduced the exact equation of phase shift and studied its relationship with phase-mismatching. The nonlinearity can be either positive or negative, depending on the sign of phase-mismatching. The induced nonlinear refractive index effectively affected the wave-vector mismatching of SHG and controlled the process. In turn, the shift of SHG spectra offered a way to measure the enhancement, which is more than three orders of magnitude higher than its intrinsic value. In addition, we used the tunable laser for our light source, by which we can choose different domain periods or wavelengths as needed to perform the experiment. Comparing with the ordinary way to control SHG by changing the temperature, our scheme also takes advantage of fast response time and large tunability.

2. MATERIALS AND METHODS

When an external electric field is applied along the y axis of a $LiNbO_3$ crystal [1], the principal axes of the new index ellipsoid rotates with an angle of $\theta \approx (\gamma_{51}E_y - s_{41}E_y^2)/[1/(n_o^\omega)^2 - 1/(n_e^\omega)^2]$ with respect to the unperturbed principal axes. Taking linear and Kerr EO effects into account, we deduce the refractive index of the new optical axis due to the equation of the index ellipsoid:

$$n_z' = n_e^{\omega} - \frac{1}{2}s_{13}(n_e^{\omega})^3 E_y^2 + \frac{1}{2}(\gamma_{51}E_y - s_{41}E_y^2)(n_e^{\omega})^3 \tan\theta, \quad (1)$$

where n_e^{ω} and n_o^{ω} represent the indices of the fundamental extraordinary and ordinary waves, γ_{51} and s_{13}, and s_{41} are the linear and quadratic electro-optic coefficients, and E_y is the y-axis external electric field, respectively. As for periodically poled $LiNbO_3$ crystal [Figs. 1(b) and 1(e)], the c axis of the $LiNbO_3$ is inverted periodically, which leads to the periodic alteration of the sign of nonlinear optical susceptibility and electro-optic coefficients. Therefore, when the electric field is applied along the y axis of PPLN, the optical axis of each domain rotates periodically, as shown in Fig. 1(a) [1,15]. Then, the energy of the incident e-polarized wave will flow to the generated o-polarized wave, and then it will flow back. If this occurs near its phase-matching condition, the returning e-polarized wave will have a different phase from the original e-polarized wave, which does not deplete completely as dedicated in Figs. 1(b) and 1(c).

Amplitude of the e-polarized wave is solved by the coupled-mode equations [1], which is $A(z) = e^{-i(\Delta\beta/2)z}[\cos(sz) + i\Delta\beta \sin(sz)/(2s)]$. $\Delta\beta = (n_o^{\omega} - n_e^{\omega})2\pi/\lambda - 2\pi/\Lambda$ is the wave-vector mismatching for cascaded linear EO effects, $s = [\kappa\kappa^* + (\Delta\beta/2)^2]^{1/2}$, κ [16] is the coupled coefficient, Λ is the domain period of PPLN, and λ is the fundamental wavelength, respectively. Then, we obtain the nonlinear phase change impressed onto the fundamental e-polarized wave at the exit surface $z = L$, which is

$$\Delta\Phi_e^{\mathrm{NL}} = \frac{\Delta\beta L}{2} - \arctan\left[\frac{\Delta\beta}{2s}\tan(sL)\right], \quad (2)$$

where L is the length of the crystal. We can also achieve an EO effective nonlinear refractive index $\Delta n_2^{\mathrm{eff}}$ deduced by $\Delta\Phi_e^{\mathrm{NL}}$, since $\Delta\Phi_e^{\mathrm{NL}} = (2\pi L/\lambda)\Delta n_2^{\mathrm{eff}}$ [17]. We plot the calculated transmission spectrum [18] and the effective EO nonlinear refractive index as a function of $\Delta\beta L$ in Fig. 2. The effective nonlinearity can be either positive or negative, depending on the sign of $\Delta\beta$. We can see that $\Delta\Phi_e^{\mathrm{NL}} > 0$, $\Delta n_2^{\mathrm{eff}} > 0$ for $\Delta\beta < 0$ and $\Delta\Phi_e^{\mathrm{NL}} < 0$, $\Delta n_2^{\mathrm{eff}} < 0$ for $\Delta\beta > 0$. It is similar to the phase shift caused by cascaded $\chi^{(2)}$:$\chi^{(2)}$ process [8,19]. $\Delta\beta = 0$ corresponds to the central fundamental wavelength λ_c of the transmission spectrum. $\Delta\beta < 0$ refers to the region that the fundamental wavelength $\lambda > \lambda_c$, and $\Delta\beta > 0$ refers to the region that $\lambda < \lambda_c$.

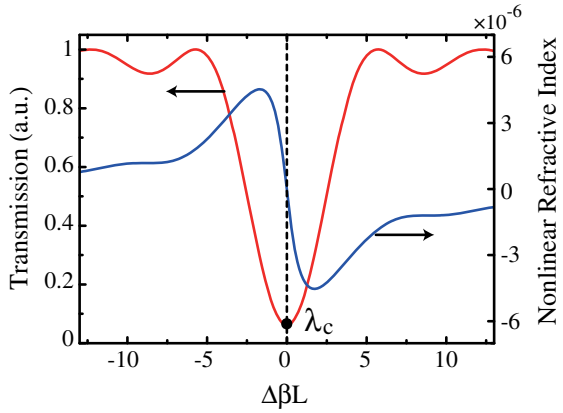

Fig. 2. Calculated transmission spectrum and the effective EO nonlinear refractive index as a function of $\Delta\beta L$. $\Delta\beta = 0$ corresponds to the central wavelength λ_c of the transmission spectrum.

In the limit of weak cascaded effects and negligible depletion of the fundamental wave, the nonlinear phase shift is approximately proportional to the square of the electric field E_y. And the effective EO nonlinear refractive index is deduced in [14] as

$$\Delta n_2^{\mathrm{eff}} \approx -\frac{2(n_o^{\omega}n_e^{\omega})^3\gamma_{51}^2}{\pi\lambda\Delta\beta}E_y^2. \quad (3)$$

Here, $|\Delta\beta| \gg |\kappa|$ should be satisfied under large phase mismatching or a low external electric field. In this case, $\Delta n_2^{\mathrm{eff}}$ is approximately proportional to the square of the external electric field and independent of the incident optical intensity.

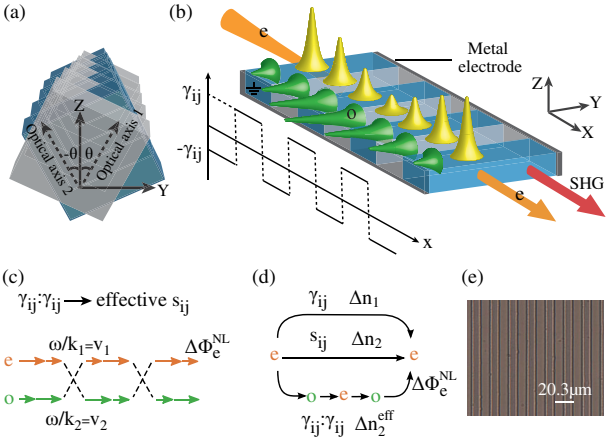

Fig. 1. (a) Rotation of the optical axes under applied y-direction external electric field. (b) Schematic of achieving cascaded linear EO effects and SHG simultaneously in a single PPLN. The periodically inverted optical axes of PPLN lead to the periodic alteration of the sign of electro-optic coefficients ($\pm\gamma_{ij}$). (c) Illustration of cascaded linear EO effects. (d) Changes of refractive indices caused by linear, Kerr, and cascaded linear EO effects, respectively. (e) Part of etched poling surface of the sample, with domain inversion period of 20.3 μm.

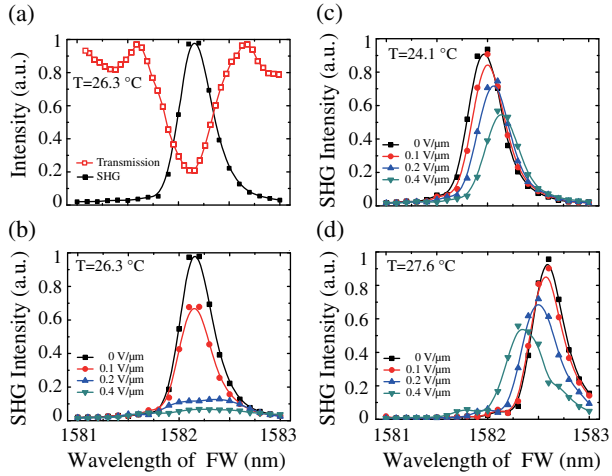

Fig. 3. (a) Measured transmission and SHG spectra fully overlapped at $T = 26.3$°C. SHG spectra with varied external electric fields at (b) 26.3°C; (c) 24.1°C; (d) 27.6°C. The intensity of SHG was modulated by the enhanced Kerr EO nonlinearity.

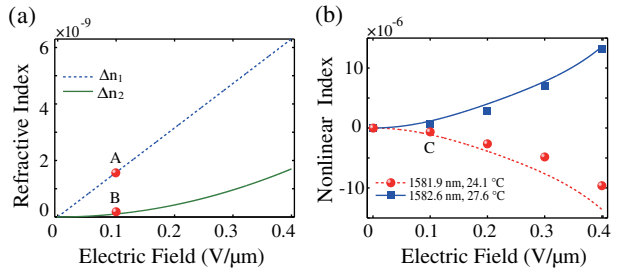

Fig. 4. (a) Index variations caused by the linear and intrinsic Kerr EO effects as a function of the external electric field. (b) Nonlinear refractive index caused by cascaded linear EO effects versus the external electric field for the specific case of $\lambda = 1581.9$ nm ($\Delta n_2^{\text{eff}} < 0$) in Fig. 3(c) and $\lambda = 1582.6$ nm ($\Delta n_2^{\text{eff}} > 0$) in Fig. 3(d). Points A, B, and C mark the index changes at 0.1 V/μm.

Otherwise, the approximation breaks down, and Eq. (3) must be solved exactly.

Thus, the index variations induced by different EO effects should be expressed by $\Delta n = \Delta n_1 + \Delta n_2 + \Delta n_2^{\text{eff}}$, as shown in Fig. 1(d). Δn_1 and Δn_2 are the changes of refractive indices by the linear and intrinsic Kerr EO effects, whose relationships with electric fields are plotted in Fig. 4(a). The EO coefficients of $LiNbO_3$ are $\gamma_{51} = 32.6 \times 10^{-12}$ m/V [1] and $s_{13} = 2.3 \times 10^{-21}$ m^2/V^2 [20], respectively. Supposing the external electric field is 0.1 V/μm ($\lambda = 1581.9$ nm, $\Delta\beta > 0$), the magnitude of the rotation angle θ is 10^{-4}. Therefore, we can obtain $\Delta n_1 = 1.6 \times 10^{-9}$, $\Delta n_2 = 1.1 \times 10^{-10}$, and $\Delta n_2^{\text{eff}} = -1.1 \times 10^{-6}$, which are marked as points A, B, and C in Fig. 4, respectively. Δn_1 and Δn_2 can be ignored if compared with Δn_2^{eff}, which makes all the index changes $\Delta n \approx \Delta n_2^{\text{eff}}$. We can obtain an effective Kerr EO coefficient, $s_{13}^{\text{eff}} = -2\Delta n_2^{\text{eff}}/[(n_e^{\omega})^3 E_y^2]$ from Eqs. (1) and (2). The calculated value is $s_{13}^{\text{eff}} \approx 2.2 \times 10^{-17}$ m^2 V^{-2}. It is more than three orders of magnitude higher than the intrinsic value [20].

For quasi-phase-matching [21,22] SHG [23,24], the wave-vector mismatching is given by $\Delta k = (n_e^{2\omega} - n_e^{\omega})4\pi/\lambda - 2\pi/\Lambda'$ with the domain period of Λ'. $n_e^{2\omega}$ is the index of second-harmonic extraordinary wave. Refractive indices are calculated by Sellmeier equations [25]. Supposing $\Lambda = \Lambda'$, the two processes can be realized in a single PPLN with a proper incident wavelength and temperature simultaneously. The induced EO nonlinear refractive index affects the original wave-vector mismatching of SHG effectively, which makes it turn into

$$\Delta k' = [n_e^{2\omega} - (n_e^{\omega} + \Delta n_2^{\text{eff}})]\frac{4\pi}{\lambda} - \frac{2\pi}{\Lambda'}. \quad (4)$$

Figure 1(e) shows one part of the etched poling surface of the z-cut 5% MgO-doped periodically poled $LiNbO_3$ crystal, with a domain inversion period of 20.3 μm and a dimension of $40 \times 10 \times 0.5$ (mm). The external electric field is applied along the y axis of PPLN, and light propagates along the x axis. The light from the tunable continuous laser (1517–1628 nm) was amplified to 100 mW (corresponding to 1.6×10^5 W/cm^2) by an erbium-doped fiber amplifier. The sample was placed between two parallel polarization beam splitters to measure the transmittance of the fundamental wave [18]. A high-voltage source with the maximum of 10 kV was used to generate the external electric field along the y axis of the PPLN. One power meter working on c-band measured the transmission of the output fundamental wave, while another power meter working on visible light measured the intensity of the second-harmonic wave, respectively.

3. RESULTS AND DISCUSSION

We observed that the two processes, namely, the cascaded linear EO effects and SHG, occurred simultaneously at the wavelength of 1582.1 nm and the same temperature of 26.3°C. The overlapped spectra are plotted in Fig. 3(a). When the experimental temperature changed, the two spectra separated from each other at an opposite direction. We measured the intensity of SHG for different external electric fields at a fixed experimental temperature. Figures 3(b)–3(d) show the results at different temperatures. The shift of the SHG spectra is due to the variable effective EO nonlinear refractive index induced by different electric fields.

As seen in Figs. 3(a) and 3(b), at 26.3°C, the absolute value $|\Delta k'|$ became larger at both sides of SHG spectrum along with the increase of the applied electric field because the spectra are fully overlapped. It led to a dramatic decrease of the SHG efficiency. At 24.1°C, as shown in Fig. 3(c), SHG spectrum is located at the left region of transmission gap ($\lambda < \lambda_c, \Delta\beta > 0$), in which $\Delta n_2^{\text{eff}} < 0$. $|\Delta k'|$ became larger at the left side and smaller at the other side of the SHG spectrum. As a result, the whole SHG spectrum moved right. Oppositely, at 27.6°C in Fig. 3(d), the SHG spectrum located at the right region of transmission gap ($\lambda > \lambda_c, \Delta\beta < 0$). The positive Δn_2^{eff} led to the SHG spectrum shifting left.

Figure 3 suggests how the enhanced Kerr EO nonlinearity controls the process of SHG. On the basis of which, we can measure the magnitude of Δn_2^{eff} according to the shift of the SHG central wavelength. The experimental results calculated from Figs. 3(c) and 3(d) are plotted in Fig. 4(b), where $\Delta n_2^{\text{eff}} < 0$ in Fig. 3(c) and $\Delta n_2^{\text{eff}} > 0$ in Fig. 3(d), respectively. They satisfy the condition of large phase-mismatching, and the variations of the effective nonlinear indices are proportional to the square of the external electric field. It is in good agreement with the simulation results deduced by Eq. (3). At $E_y = 0.1$ V/μm (1581.9 nm, $\Delta\beta > 0$), the experimental values are $\Delta n_2^{\text{eff}} = -6.4 \times 10^{-7}$, and we obtain $s_{13}^{\text{eff}} \approx 1.3 \times 10^{-17}$ m^2 V^{-2}, which are identical to the theoretical values.

In general, there are three other possible effects that may contribute to the shift of the SHG spectra, including the intensity of the fundamental light, the index change caused by intrinsic EO effects, and the cascaded nonlinearity between the second-harmonic and fundamental wave. However, in our scheme, all of them are not possible to come into play.

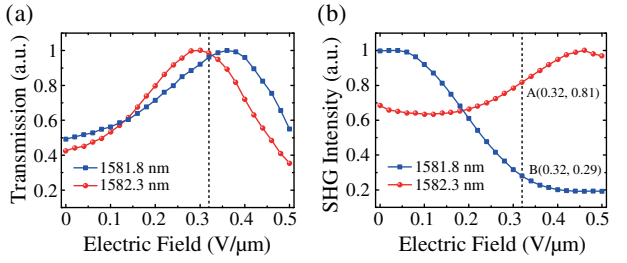

Fig. 5. Measured normalized transmission (a) and SHG intensity (b) at two selected wavelengths [1581.8 and 1582.3 nm in Fig. 3(c)] as a function of the external electric fields. At $E_y = 0.32$ V/μm, the two wavelengths have the same transmittances but quite different SHG intensities.

First, since the intensity of SHG is proportional to the square of the intensity of the fundamental wave [2], we observed the normalized transmission and SHG intensity as a function of the applied electric field. As demonstrated in Fig. 5, we selected two wavelengths of 1581.8 and 1582.3 nm from each sideband of the SHG spectrum in Fig. 3(c). At $E_y = 0.32$ V/μm, the same normalized transmittances were measured for these two different wavelengths. However, for their normalized SHG intensities, the one is high to 0.81 at A and the other is low to 0.29 at B. It means that, although the intensity of incident light varies with the external electric field, it hardly affects the efficiency of SHG. Second, when the temperature was high enough that the transmission spectrum is barely overlapped with SHG, we observed that the SHG spectrum remained unchanged when varying the external electric fields. It agrees well with our discussion that the index variation caused by intrinsic EO effects are small, so it can be neglected. Last, the cascaded second-order nonlinear process is invalid in this case because the incident optical intensity is pretty low (1.6×10^5 W/cm^2).

We also observed the same phenomena at domain periods of 20.1 and 19.9 μm, which makes it significant to explore the further intrinsic bond between the two physical processes. The wave-vector mismatchings are determined by the dispersion relations [25], as a function of the wavelength, domain inversion period, and temperature. Supposing $\Delta\beta$ and Δk equal to 0 simultaneously, the relationship between the domain period and wavelength is plotted in Fig. 6. Points a, b, and c correspond to the three inversion domain periods we performed in our experiment. The inaccuracy of Sellmeier equations causes the theoretical wavelength (1583.1 nm) for 20.3 μm, which is a little shift from the experimental condition (1582.1 nm). By careful calculation, we confirm that these two processes can be satisfied simultaneously at a designed domain inversion period if employing a proper wavelength and temperature. The corresponding relationship is inserted in Fig. 6. Therefore, if given one of the three parameters in Fig. 6, we can find the other two, which is significant in practical flexibility and adjustability.

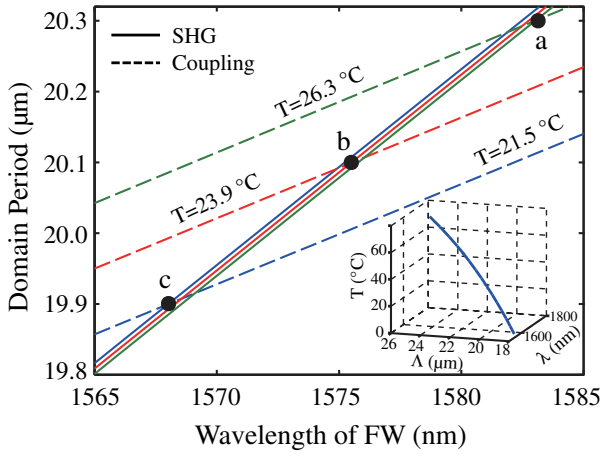

Fig. 6. Calculated inversion domain periods for achieving SHG (solid) and the cascading effects (dashed) as a function of fundamental wavelengths at different temperatures. Points a, b, and c correspond to the three inversion domain periods we performed in our experiment. Inset figure shows the relationship among the three parameters to realize the cascading process and SHG simultaneously.

4. CONCLUSIONS

In conclusion, we demonstrated a new scheme of manipulating the second-order nonlinear effect by enhanced Kerr EO nonlinearity. The enhanced Kerr EO nonlinearity is more than three orders of magnitude higher than the intrinsic value. Moreover, besides SHG, other second-order parametric processes such as sum and difference frequency generation can also be manipulated by this enhanced Kerr EO nonlinearity. The principal basis of this Kerr EO nonlinearity is quite different from that induced by cascaded second-order nonlinear processes, for its independence of the light intensity. Therefore, it can find potential applications in electrically controlled third-order nonlinearities, such as group velocity control, phase modulation, etc.

ACKNOWLEDGMENT

The research was supported by the National Natural Science Foundation of China under Grant Nos. 11174204, 61125503, and 61235009.

REFERENCES

1. A. Yariv and P. Yeh, *Optical Waves in Crystals* (Wiley, 1984), Vol. **8**.
2. R. W. Boyd, *Nonlinear Optics* (Academic, 2003).
3. B. Daino, G. Gregori, and S. Wabnitz, "New all-optical devices based on third-order nonlinearity of birefringent fibers," Opt. Lett. **11**, 42–44 (1986).
4. E. C. Stevenson and J. W. Beams, "The electro-optical kerr effect in gases," Phys. Rev. **38**, 133–140 (1931).
5. M. Melnichuk and L. T. Wood, "Direct Kerr electro-optic effect in noncentrosymmetric materials," Phys. Rev. A **82**, 013821 (2010).
6. C. Kolleck, "Cascaded second-order contribution to the third-order nonlinear susceptibility," Phys. Rev. A **69**, 053812 (2004).
7. D. Wang, Y. Zhang, and M. Xiao, "Quantum limits for cascaded optical parametric amplifiers," Phys. Rev. A **87**, 023834 (2013).
8. G. I. Stegeman, D. J. Hagan, and L. Torner, "χ (2) cascading phenomena and their applications to all-optical signal processing, mode-locking, pulse compression and solitons," Opt. Quantum Electron. **28**, 1691–1740 (1996).
9. C. Bosshard, R. Spreiter, M. Zgonik, and P. Günter, "Kerr nonlinearity via cascaded optical rectification and the linear electro-optic effect," Phys. Rev. Lett. **74**, 2816–2819 (1995).
10. T. Z. Shen, S. H. Hong, and J. K. Song, "Electro-optical switching of graphene oxide liquid crystals with an extremely large kerr coefficient," Nat. Mater. **13**, 394–399 (2014).
11. R. L. Jin, Y. H. Yu, H. Yang, F. Zhu, Q. D. Chen, M. B. Yi, and H. B. Sun, "Electro-optical detection based on large kerr effect in polymer-stabilized liquid crystals," Opt. Lett. **37**, 842–844 (2012).
12. Y. Hisakado, H. Kikuchi, T. Nagamura, and T. Kajiyama, "Large electro-optic kerr effect in polymer-stabilized liquid-crystalline blue phases," Adv. Mater. **17**, 96–98 (2005).
13. M. G. Kuzyk, J. E. Sohn, and C. W. Dirk, "Mechanisms of quadratic electro-optic modulation of dye-doped polymer systems," J. Opt. Soc. Am. B **7**, 842–858 (1990).
14. J. Huo and X. F. Chen, "Large phase shift via polarization-coupling cascading," Opt. Express **20**, 13419–13424 (2012).
15. Y. Q. Lu, Z. L. Wan, Q. Wang, Y. X. Xi, and N. B. Ming, "Electro-optic effect of periodically poled optical superlattice linbo$_3$ and its applications," Appl. Phys. Lett. **77**, 3719–3721 (2000).
16. K. Liu, W. J. Lu, Y. P. Chen, and X. F. Chen, "Active control of group velocity by use of folded dielectric axes structures," Appl. Phys. Lett. **97**, 071104 (2010).
17. Y. Shen, T. Watanabe, D. A. Arena, C. C. Kao, J. B. Murphy, T. Y. Tsang, X. J. Wang, and G. L. Carr, "Nonlinear cross-phase modulation with intense single-cycle terahertz pulses," Phys. Rev. Lett. **99**, 043901 (2007).

18. X. F. Chen, J. H. Shi, Y. P. Chen, Y. M. Zhu, Y. X. Xia, and Y. L. Chen, "Electro-optic solc-type wavelength filter in periodically poled lithium niobate," Opt. Lett. **28**, 2115–2117 (2003).
19. R. DeSalvo, H. Vanherzeele, D. J. Hagan, M. Sheik-Bahae, G. Stegeman, and E. W. Van Stryland, "Self-focusing and self-defocusing by cascaded second-order effects in ktp," Opt. Lett. **17**, 28–30 (1992).
20. M. Luennemann, U. Hartwig, G. Panotopoulos, and K. Buse, "Electrooptic properties of lithium niobate crystals for extremely high external electric fields," Appl. Phys. B **76**, 403–406 (2003).
21. J. Xie, Y. Chen, W. Lu, and X. Chen, "Bidirectionally tunable all-optical switch based on multiple nano-structured resonators using backward quasi-phase-matching," Chin. Opt. Lett. **9**, 041902 (2011).
22. X. P. Hu, P. Xu, and S. N. Zhu, "Engineered quasi-phase-matching for laser techniques invited," Photon. Res. **1**, 171–185 (2013).
23. Y. P. Chen, R. Wu, X. L. Zeng, Y. X. Xia, and X. F. Chen, "Type i quasi-phase-matched blue second harmonic generation with different polarizations in periodically poled $linbo_3$," Opt. Laser Technol. **38**, 19–22 (2006).
24. J. F. Zhang, Y. P. Chen, F. Lu, and X. F. Chen, "Flexible wavelength conversion via cascaded second order nonlinearity using broadband shg in mgo-doped ppln," Opt. Express **16**, 6957–6962 (2008).
25. O. Gayer, Z. Sacks, E. Galun, and A. Arie, "Temperature and wavelength dependent refractive index equations for mgo-doped congruent and stoichiometric $linbo_3$," Appl. Phys. B **91**, 343–348 (2008).